Accepted Manuscript

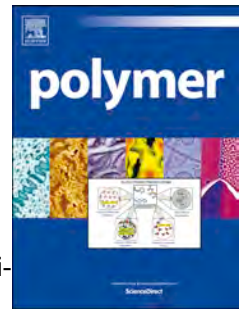

Confinement effects in one-dimensional nanoarrays of polymer semiconductors and their photovoltaic blends

Jaime J. Hernández, Inés Puente-Orench, Tiberio A. Ezquerra, Edgar Gutiérrez, Mari-Cruz García-Gutiérrez

PII: S0032-3861(18)31150-9

DOI: https://doi.org/10.1016/j.polymer.2018.12.036

Reference: JPOL 21123

To appear in: *Polymer*

Received Date: 30 August 2018

Revised Date: 3 December 2018

Accepted Date: 24 December 2018

Please cite this article as: Hernández JJ, Puente-Orench Iné, Ezquerra TA, Gutiérrez E, García-Gutiérrez M-C, Confinement effects in one-dimensional nanoarrays of polymer semiconductors and their photovoltaic blends, *Polymer* (2019), doi: https://doi.org/10.1016/j.polymer.2018.12.036.

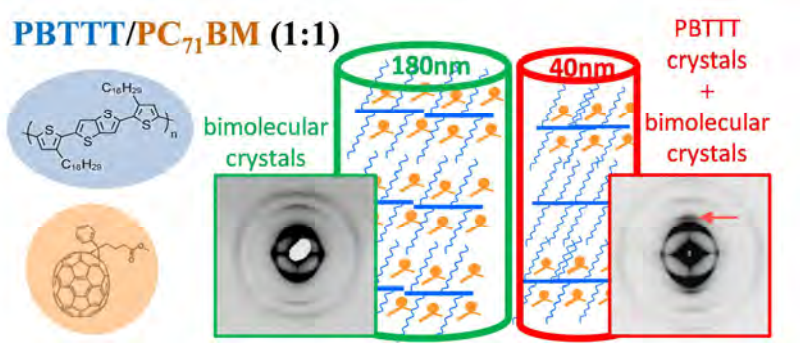

Confinement effects in one-dimensional nanoarrays of polymer semiconductors and their photovoltaic blends

Jaime J. Hernández [a], Inés Puente-Orench [b,c] , Tiberio A. Ezquerra[d], Edgar Gutiérrez[d], Mari-Cruz García-Gutiérrez*[,d]

[a]Institute for Advanced Studies in Nanoscience, Faraday 9, 28049 Madrid, Spain

[b]Aragón Materials Science Institute, Pedro Cerbuna 12, 50009 Zaragoza, Spain

[c]Institut Laue-Langevin, 71 av. des Martyrs, 38042 Grenoble Cedex 9, France.

[d]Institute for the Structure of Matter (IEM-CSIC), Serrano 121, 28006 Madrid, Spain

Keywords: confinement; conjugated polymers; X-ray nanoprobes; nanowires; organic electronics.

Corresponding Author

*E-mail: maricruz@iem.cfmac.csic.es

ABSTRACT

We report on the strong changes induced, by confinement, in the microstructure of the semiconductor poly(2,5-bis(3-hexadecylthiophen-2-yl)thieno[3,2-b]thiophene) (PBTTT) and its photovoltaic blend with [6,6]-Phenyl-C71-butyric acid methyl ester ($PC_{71}BM$). These organic compounds can be used as model systems to illustrate how sensitive this class of materials can be to spatial confinement on device-relevant length scales. The spatial confinement of

nanofilaments as a function of diameter, from 180 to 25 nm, has been investigated by X-ray scattering with nanofocused synchrotron beams. The effects of spatial confinement are evident by crystallization in different crystal forms, reduction of crystallinity, phase segregation and anisotropic crystal orientation. It is also shown that confinement is an efficient tool to direct the overall texture included the crystal orientation of the homopolymer PBTTT and the PBTTT/$PC_{71}BM$ blend in a controlled manner.

1. Introduction

The solution processable semiconductor polymers and small molecules are extensively investigated for applications in organic electronics, due to their attractive opportunities for the fabrication of low-cost, flexible and large area electronics [1-4]. In particular the poly(2,5-bis(3-hexadecylthiophen-2-yl)thieno[3,2-b]thiophene) (PBTTT) has been already implemented in organic field-effect transistors (OFETs) [5, 6], organic photovoltaics (OPVs) [7, 8] and organic thermoelectrics [9]. All of these devices are based on architectures where organic semiconductors are confined to small spatial volumes [1, 10]. In particular efficient polymer solar cells use a bulk-heterojunction (BHJ) photoactive layer, where a nanosized phase-separated blend of electron-donating and electron-accepting semiconductors provides extensive interface areas for efficient exciton dissociation and a connected pathway for charge transport [11]. Power conversion efficiencies (PCEs) higher than 11% have been reported for polymer/fullerene BHJ solar cells [12, 13]. In addition, the microstructure and the phase separation between the blend components in the BHJ play an important role in the OPV device performance [14-16]. One approach to improve light harvesting is the adjustment of the photoactive layer with periodic structures [17]. Nanoimprint lithography (NIL) [18, 19] and laser-induced periodic surface structures (LIPSS) [20-22] have been used to produce controlled nanostructures for OPV

applications. While the methods of NIL and LIPSS have been employed to fabricate low aspect ratio nanostructures, the advantage of the template wetting procedure, using porous anodic aluminum oxide (AAO) as a template, is the versatility of the technique, enabling the fabrication of customized polymer nanorods comprising high aspect ratio (length/diameter) one-dimensional (1D) nanostructures both by melt and solution wetting [23-26]. Moreover, X-ray scattering with micro- and nano-focused synchrotron beams allows for studying size-dependent processes with length scales comparable to the nanostructures' size in 1D nanostructures [27, 28]. Indeed, polymer crystallization under confinement is an example of phenomena that can deviate considerably from the respective dependencies observed in bulk [29, 30], as it is known that crystal nucleation [31, 32], growth and orientation [25, 31, 33] are influenced by size limitation at the nanometer scale. In the studied case of PBTTT, the high carrier mobility is due to both the material's inherent crystallinity and the well oriented crystallites within the nanostructures, being the orientation of the entities which facilitate charges to easily travel between neighboring crystalline domains. It has been reported that for PBTTT thin films thinner than 20 nm the crystallinity is strongly inhibited and the charge carrier mobility drops due to the decrease in crystalline fraction [34]. For films thicker than 20 nm, with abundance of crystallites, the number of percolating paths is controlled by crystalline texture. But in the case of low crystallinity, the number of percolating paths is controlled by crystallite density. This implies that the different filament size-dependence of these two factors (crystallite density and crystallite orientation) would lead to an optimal PBTTT filament size at which mobility is maximized. It has been also reported that the PBTTT hole mobility decreases an order-of-magnitude upon the addition of $PC_{71}BM$, what can be attributed not only to the dilution of the hole-transporting material, but also to the disruption of the polymer π-stacking that results both from the backbone twists and

the additional unit-cell volume required to account for the intercalated fullerene [6, 35]. This problem could be solved by inducing phase separation in the blend by nanoconfinement in ordered nanostructures, if the domain sizes can be maintained on the tens of nanometer since the exciton diffusion length in the conjugated polymer is limited to ~10 nm [36].

In the present work, we elucidate the changes induced, by confinement, in the microstructure of the PBTTT conjugated polymer and its photovoltaic blend with [6,6]-Phenyl-C71-butyric acid methyl ester ($PC_{71}BM$) as model systems on device-relevant length scales.

2. Experimental section

2.1. Materials and sample preparation

Poly(2,5-bis(3-hexadecylthiophen-2-yl)thieno[3,2-b]thiophene) with $–C_{16}H_{29}$ side chains (PBTTT) and [6,6]-Phenyl-C71-butyric acid methyl ester ($PC_{71}BM$) were purchased from Ossila. PBTTT (Batch M141, molecular weight of M_w = 82800 g/mol and polydispersity of M_w/M_n = 2.68), $PC_{71}BM$ (Batch M114, molecular weight of M_w = 1031 g/mol and a purity of 99%). The chemical structures of PBTTT and $PC_{71}BM$ are presented in Figure S1.

Hexagonally ordered AAO templates with pores of 25, 40 and 180 nm in diameter (Figure S2) were purchased from SmartMembranes. The cross-sectional images of the templates (Figure S3) demonstrate that the pores are straight and homogeneous in diameter. The pore depth is ~55 μm. The membranes were washed applying ultrasound after submerging them in hexane. The solution wetting method [37] was used in order to infiltrate PBTTT and the blend PBTTT/ $PC_{71}BM$ into the AAO templates. For neat PBTTT 65 mg of PBTTT was dissolved in 1 mL of dichlorobenzene, the PBTTT solution was heated to 80 ºC with agitating. The blend of PBTTT and $PC_{71}BM$ with a ratio of 1:1 was prepared dissolving separately 65 mg of both PBTTT and

$PC_{71}BM$ in 1mL of dichlorobenzene each of them, the blend solution was also heated to 80 ºC with stirring. The AAO membranes are covered by the polymer solution and during 4 hours are kept at 80 ºC in order to avoid PBTTT gels [38]. Afterwards they are dried under vacuum at room temperature for 24 hours. All the infiltrated templates were finally annealed at 180 ºC for 20 min [6, 39]. The measured residual polymer films on the top of the infiltrated membranes have a thickness in the range 6-18 μm.

2.2. Characterization

Scanning electron microscopy. The surface, the average pore size and the lateral size of the AAO membranes were characterized from the images of combined secondary and backscattered electrons acquired by a Hitachi S-8000 scanning electron microscope working at 0.5 kV to minimize sample damage.

Structural characterization by means of scanning X-ray micro-diffraction. X-ray diffraction with a nano-focused synchrotron beam of 400 nm diameter and a wavelength of λ= 0.0832 nm has been carried out at the Microfocus beamline (ID13) at the European Synchrotron Radiation Facility (ESRF). Slides of 1 mm wide were cut from the infiltrated membranes, mounted horizontally with the nanopore axis carefully aligned perpendicular to the X-ray beam (Figure 1) and scanning X-ray micro-diffraction (μ-XRD) with steps of 1 μm was performed along the main axis of the pores, from the residual film (bulk) outside the membrane to the infiltrated material (Figure 1). The 2D diffraction patterns were registered in transmission geometry using a FReLoN detector (2048 x 2048 pixels of 51.47 x 50.7 μm^2; 16-bit readout). A sample-to detector distance of D = 147 mm was calibrated using an Ag-behenate standard and the small- and wide-angle X-ray scattering

(SAXS and WAXS) intensities were accessible in the same pattern. The data analysis was accomplished using the software Fit2D [40].

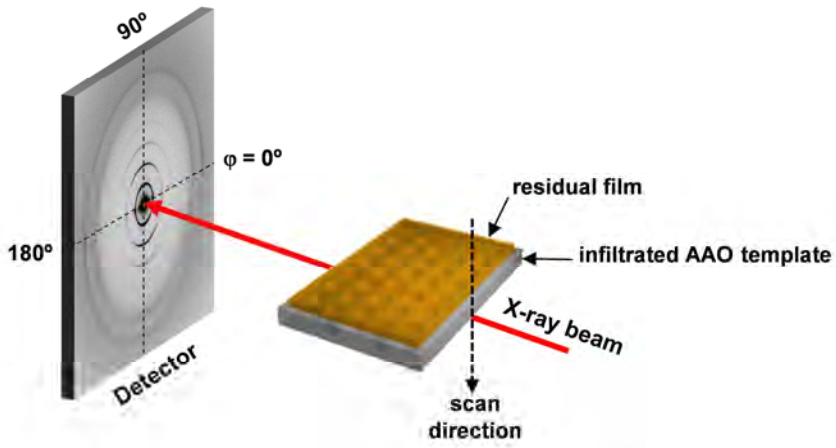

Figure 1. Schematic view of a scanning μ-XRD experiment showing the convention for the azimuthal angle φ adopted in this work.

3. Results and discussion

3.1. PBTTT

High aspect ratio 1D nanoarrays of PBTTT and the blend PBTTT/ $PC_{71}BM$ (1:1) supported by a residual film have been fabricated infiltrating AAO templates based on the wettability of high surface energy inorganic materials (AAO) by low surface energy polymer solutions [25].

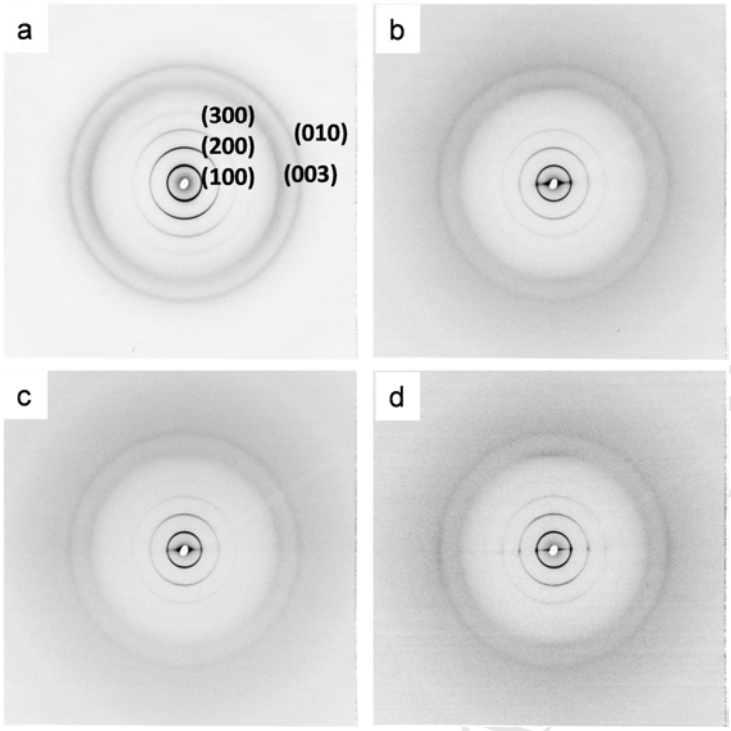

Figure 2. 2D X-ray diffraction patterns: Residual PBTTT film (a). PBTTT nanofilaments inside porous alumina of 25 nm (b), 40 nm (c) and 180 nm (d) pore diameter. The Miller indices of the main reflections are labeled.

PBTTT nanostrucure has been studied by X-ray scattering. With the above mentioned set-up, SAXS and WAXS signals are obtained simultaneously. Figure 2(a) displays the 2D diffraction pattern of the residual PBTTT film and Figure 2(b), 2(c) and 2(d) show those of the PBTTT nanofilaments inside porous alumina of 25 nm, 40 nm and 180 nm pore diameter respectively. The WAXS signal from the PBTTT nanofilaments with different diameters and also from the residual PBTTT film appear slightly oriented (Figure 2). However, while the pattern corresponding to the residual PBTTT film doesn't present any SAXS feature close to the beam stop, the infiltrated material (Figure 2(b), 2(c) and 2(d)) exhibit a continuous, oriented SAXS signal on the equator related to correlation lengths corresponding to the pores of the AAO

template and not to the polymer [25, 37, 41]. The SAXS feature is accompanied at wide angles by a broad amorphous halo also related to the AAO membrane [37, 41].

The evolution of the integrated 1D scattered intensity as a function of the modulus of the scattering vector s ($s = 2\sin(\theta)/\lambda$) , from the residual PBTTT film to the nanofilaments into the AAO pores of 40 nm diameter (Figure 3(a)) shows that no crystal phase transition is induced by confinement. Therefore the 1D intensity profile as a function of s has been obtained by the projection of the integrated scattered intensity in Figure 3a through all the positions (Figure 3(b)). The experimental d spacing ($d = 1/s$) obtained are as follows: $d_{(100)}$= 23.0 Å, $d_{(200)}$= 11.4 Å, $d_{(300)}$= 7.6 Å, $d_{(003)}$= 4.3 Å, $d_{(010)}$= 3.6 Å. These values are in agreement with the calculated values taking into account a triclinic unit cell that has been previously reported for PBTTT with $-C_{16}H_{29}$ side chains: a = 23.5 Å, b = 5.4 Å, c = 13.5 Å, α = 137°, β= 87º and γ= 92º [42].

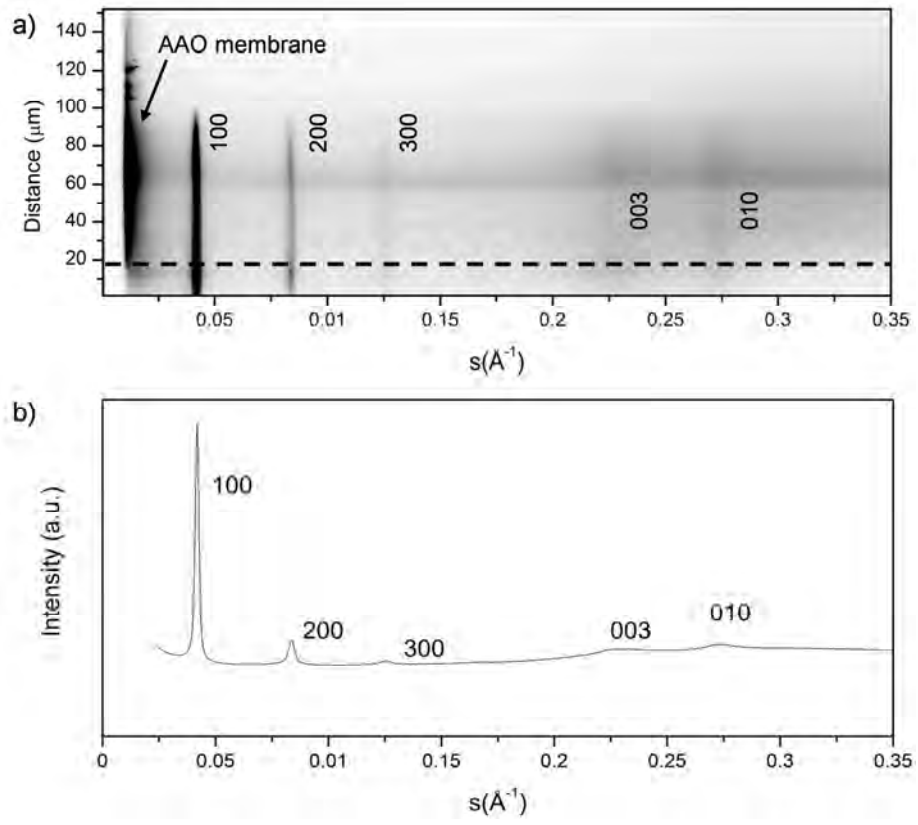

Figure 3. (a) Integrated 1D scattered intensity of PBTTT as a function of the modulus of the scattering vector s and the distance from the residual film to the nanofilaments into AAO pores of 40 nm along the pore axis. The dashed line indicates the boundary between the residual film and the nanofilaments into the AAO template. (b) Projected 1D intensity as a function of s.

The azimuthal integration, i.e., with respect to angle φ (presented in Figure 1), gives 1D intensity profiles that can provide insights regarding the crystal orientation of PBTTT. Figure 4 shows the normalized integrated intensity of the 200 reflection as a function of the azimuthal angle (φ) for the residual film and the nanofilaments into AAO pores with diameters of 25 and 180 nm. The 200 reflection has been selected instead of the more intense 100 reflection in order to avoid the contribution of the equatorial streak coming from the AAO membrane. The PBTTT residual film presents an intensity profile with a broad maximum centered at φ = 90º (meridian) indicating that the *a*-axis of the crystal unit cell is preferentially aligned perpendicular to the surface of the AAO membrane (free of pores) with the *c*-axis (which corresponds to the polymer backbone direction) parallel to the surface of the AAO membrane. This orientation is similar to the one of PBTTT thin films on silicon substrates [42]. The PBTTT nanofilaments present intensity profiles exhibiting an extra intensity maximum centered at φ = 0º and at φ = 180º (equator) being this maximum more prominent for the nanofilaments with bigger diameter. This new intensity maximum centered at the equator indicates that the crystals in the PBTTT nanofilaments tend to orient concentric to each other with the *a*-axis perpendicular to the AAO nanochannel surface and pore axis due to the strong interaction of the polymer with the pore walls as previously observed for other polymers [32, 37, 41].

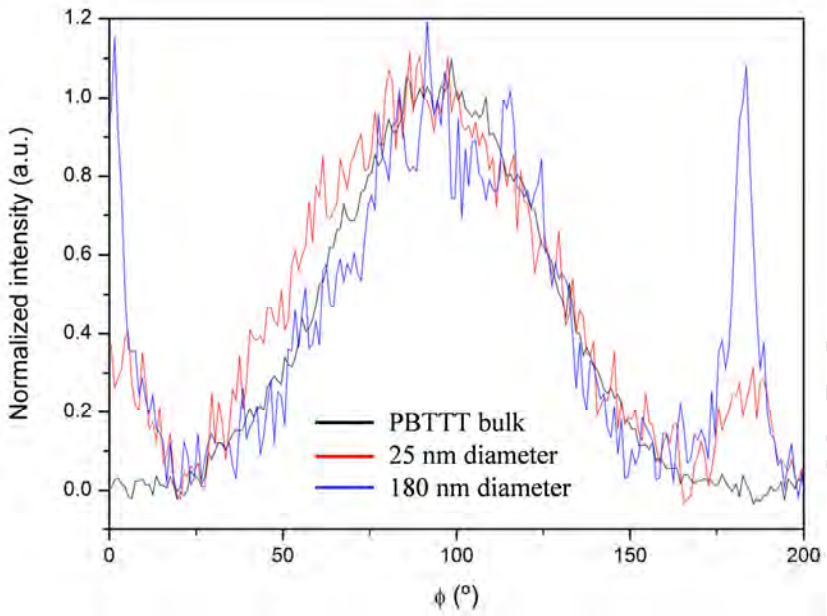

Figure 4. Normalized integrated intensity of the 200 reflection as a function of the azimuthal angle (φ) for the residual film (black), the nanofilaments inside AAO pores of 25 nm diameter (red) and the nanofilaments inside AAO pores of 180 nm diameter (blue).

3.2. PBTTT/ $PC_{71}BM$ (1:1) blend

High aspect 1D nanoarrays of the blend PBTTT/ $PC_{71}BM$ (1:1) with diameters of 25, 40 and 180 nm have also been fabricated by solution template wetting. Figure 5(a) exhibits the 2D diffraction pattern of the residual PBTTT/ $PC_{71}BM$ film and Figure 5(b) that of the PBTTT/ $PC_{71}BM$ nanofilaments inside porous alumina of 180 nm pore diameter. While no new reflections are generated due to confinement, a slightly different orientation is observed by comparing both patterns.

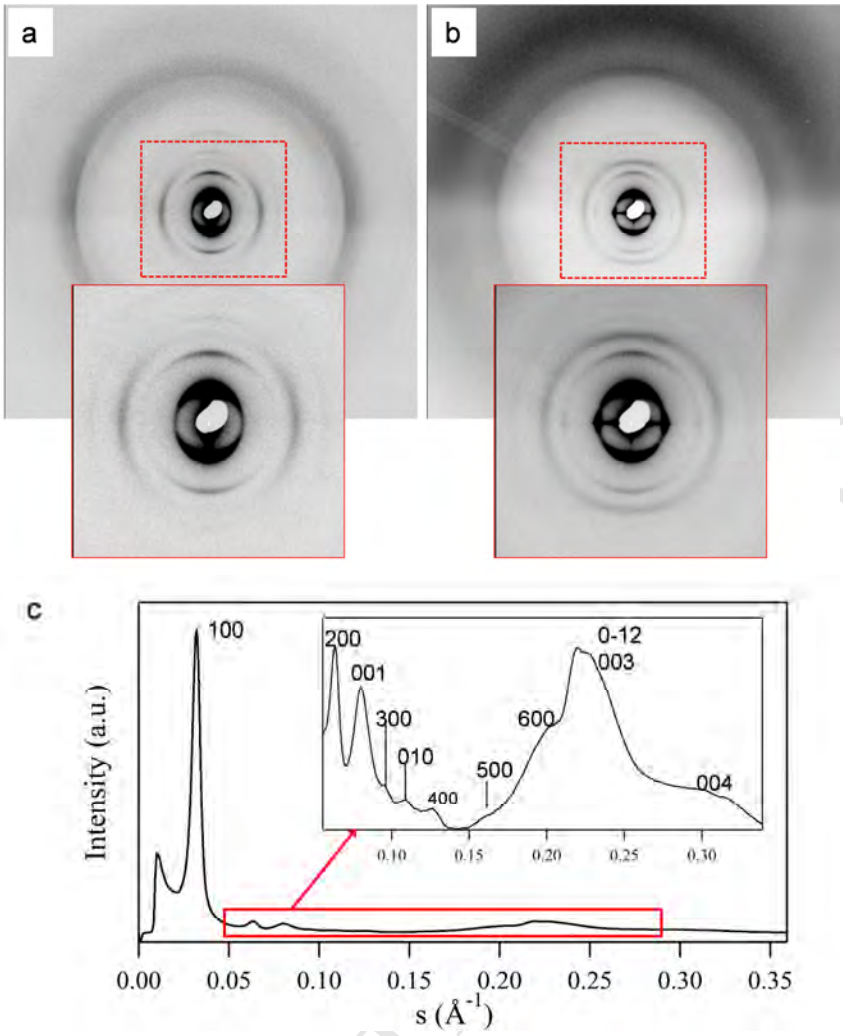

Figure 5. 2D X-ray diffraction patterns of the PBTTT/$PC_{71}BM$ (1:1) blend: Residual PBTTT/$PC_{71}BM$ (1:1) film (a) and PBTTT/PCBM (1:1) nanofilaments inside AAO pores of 180 nm diameter (b). The central area of the patterns has been augmented and shown as insets. (c) 1D intensity profile as a function of the modulus of the scattering vector s, for the PBTTT/$PC_{71}BM$ (1:1) nanopillars inside AAO pores of 180 nm diameter. Part of the intensity profile has been enlarged and presented as an inset.

The one dimensional scattered intensity profile as a function of the scattering vector, s, was extracted from the 2D patterns by performing a radial integration using the whole azimuthal

range (Figure 5(c)). In order to index the series of reflections we took into account a monoclinic unit cell previously reported for PBTTT/$PC_{71}BM$ (1:1) thin films.[43] The monoclinic unit cell contains one PBTTT monomer per fullerene molecule, considering that bimolecular crystals form due to the intercalation of the fullerene derivative in the polymer network [43]. The monoclinic unit-cell with the following parameters a = 31 Å, b = 10 Å, c = 13.5 Å, α = 108°, β= 90º and γ= 90º is compatible with all the observed reflections, as indicated in Table 1.

Table 1. Experimental (d_{exp}) and calculated (d_{calc}) d spacings of PBTTT/$PC_{71}BM$ (1:1) residual film and nanofilaments inside AAO pores of 180 nm diameter. The values of d_{exp} are derived from the 1D intensity profile given in Figure 5(c).

hkl	**d_{exp} (Å)**	**d_{calc} (Å)**
100	31.4	31.0
200	15.8	15.5
001	12.5	12.8
300	10.7	10.3
010	9.3	9.5
400	7.9	7.8
500	6.3	6.2
600	5.0	5.1
0-13	4.5	4.5
003	4.4	4.3
004	3.3	3.2

Figure 6 shows the 2D diffraction pattern of the PBTTT/ $PC_{71}BM$ nanofilaments into AAO porous of 40 nm pore diameter. Two new reflections, indicated by arrows, are observed comparing this diffraction pattern to those in Figure 5 corresponding to a residual

PBTTT/$PC_{71}BM$ (1:1) film and PBTTT/$PC_{71}BM$ (1:1) nanofilaments inside AAO pores of 180 nm diameter. In Figure S4 it is clearly observed that the new reflections appear for the material infiltrated in the nanopores but they are not present in the residual film.

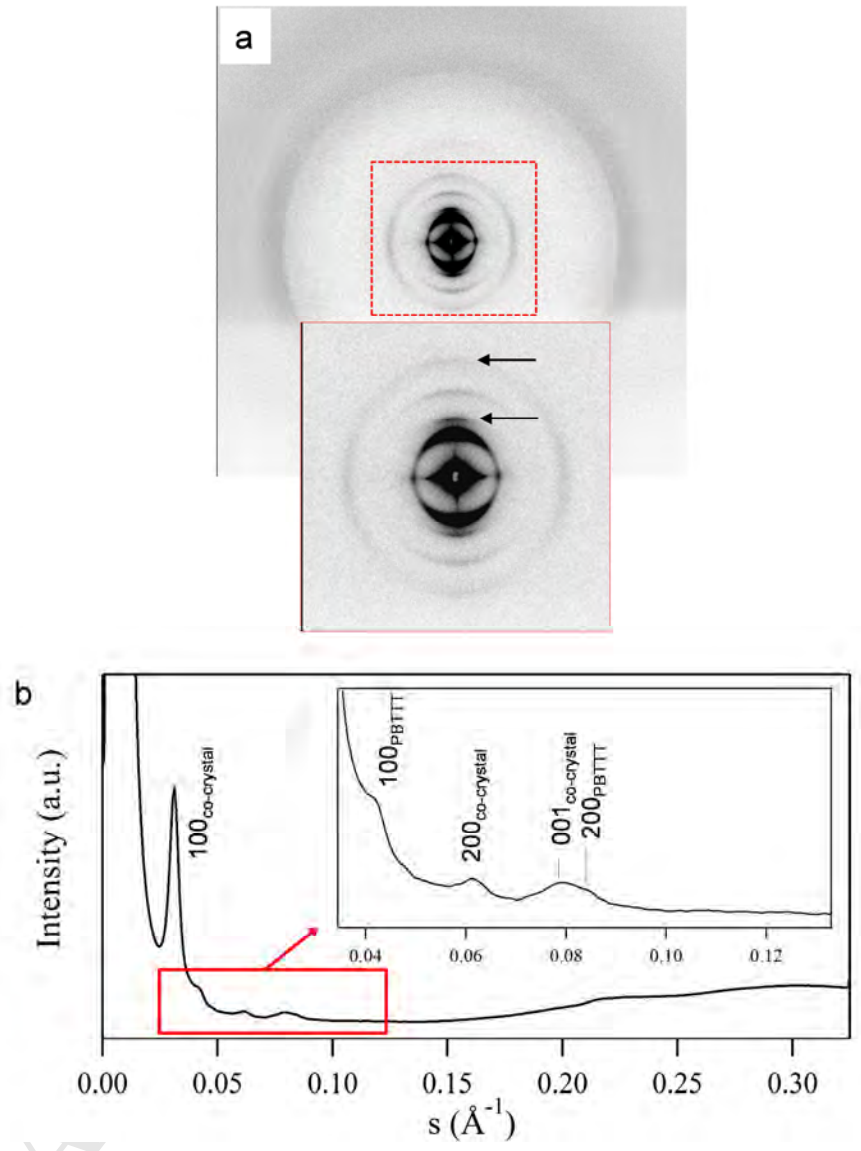

Figure 6. (a) 2D X-ray diffraction patterns of PBTTT/$PC_{71}BM$ (1:1) nanofilaments inside AAO pores of 40 nm diameter. The central area of the patterns has been augmented and shown as inset. Arrows in the inset indicate new reflections absent in the pattern of the PBTTT/$PC_{71}BM$

(1:1) residual film (Figure 5a). (b) 1D intensity profile as a function of the modulus of the scattering vector s, for the PBTTT/$PC_{71}BM$ (1:1) nanofilaments inside AAO pores of 40 nm diameter. Part of the intensity profile has been enlarged and presented as an inset.

In order to elucidate the nature of the new reflections, the 1D intensity profile as a function of s has been extracted from the 2D pattern (Figure 6(b)). And we have derived from it the experimental d spacing of the intensity maxima (Table 2). Most of the reflections present d spacing corresponding to the calculated d spacing taking into account the previous monoclinic unit cell considering the co-crystallization of PBTTT and $PC_{71}BM$. Although two of the reflections cannot be indexed considering this monoclinic unit cell, however their measured d spacing agrees with the calculated d spacing of the most intense reflections of PBTTT (100 and 200) taking into account the triclinic unit cell previously reported for PBTTT [42]. These results suggest that the confinement of PBTTT/$PC_{71}BM$ (1:1) inside AAO pores of 40 nm diameter induces partial phase segregation provoking two different crystal populations. One of them corresponding to PBTTT crystals with a triclinic unit cell (a = 23.5 Å, b = 5.4 Å, c = 13.5 Å, α = 137°, β= 87º and γ= 92º) and the other corresponding to the co-crystallization of PBTTT and $PC_{71}BM$ with a monoclinic unit-cell (a = 31 Å, b = 10 Å, c = 13.5 Å, α = 108°, β= 90º and γ= 90º). The absence of reflections corresponding to $PC_{71}BM$ crystals could indicate either that an amorphous phase of the blend rich in $PC_{71}BM$ is present into the 40 nm AAO pores, or that a fraction of $PC_{71}BM$ molecules is not infiltrated into the AAO pores. The second option would imply an excess of $PC_{71}BM$ in the residual film outside the AAO membrane. It has been published that blends with an excess of $PC_{71}BM$ show reflections from the bimolecular crystal and pure $PC_{71}BM$.[43] In our case no diffraction from pure $PC_{71}BM$ is observed in the residual

film (Figure S5) then we can conclude that $PC_{71}BM$ is infiltrated into the AAO pores and the nanofilaments present an amorphous phase rich in $PC_{71}BM$.

Table 2. Experimental (d_{exp}) and calculated (d_{calc}) d spacing of PBTTT/$PC_{71}BM$ (1:1) nanofilaments inside AAO pores of 40 nm diameter. The values of d_{exp} are derived from the 1D intensity profile given in Figure 6.

hkl	**d_{exp} (Å)**	**d_{calc} (Å)**
$100_{co\text{-}crystal}$	31.8	31.0
100_{PBTTT}	23.6	23.4
$200_{co\text{-}crystal}$	16.2	15.5
$001_{co\text{-}crystal}$	12.8	12.8
200_{PBTTT}	11.4	11.7

Figure 7(a) shows the 2D diffraction pattern of the PBTTT/ $PC_{71}BM$ nanofilaments into AAO porous of 25 nm diameter. In order to increase the weak intensity of the reflections Figure 7(a) is the addition of 10 patterns taken with 1micron step along the AAO pore axis. The 1D intensity profile as a function of s (Figure 7(b)) has been obtained by the integration of the scattered intensity considering the section drawn in the inset of Figure 7(a). In order to get the d spacing of the two observed reflections an exponential background (red dashed line in Figure 7(b)) has been subtracted from the 1D intensity profile. The result is presented as an inset in Figure 7(b). The experimental d spacing obtained are as follows: $d_{(100)}$= 23.8 Å, $d_{(200)}$= 12.3 Å. These values are in agreement with the calculated values taking into account a triclinic unit cell that has been previously reported for PBTTT.

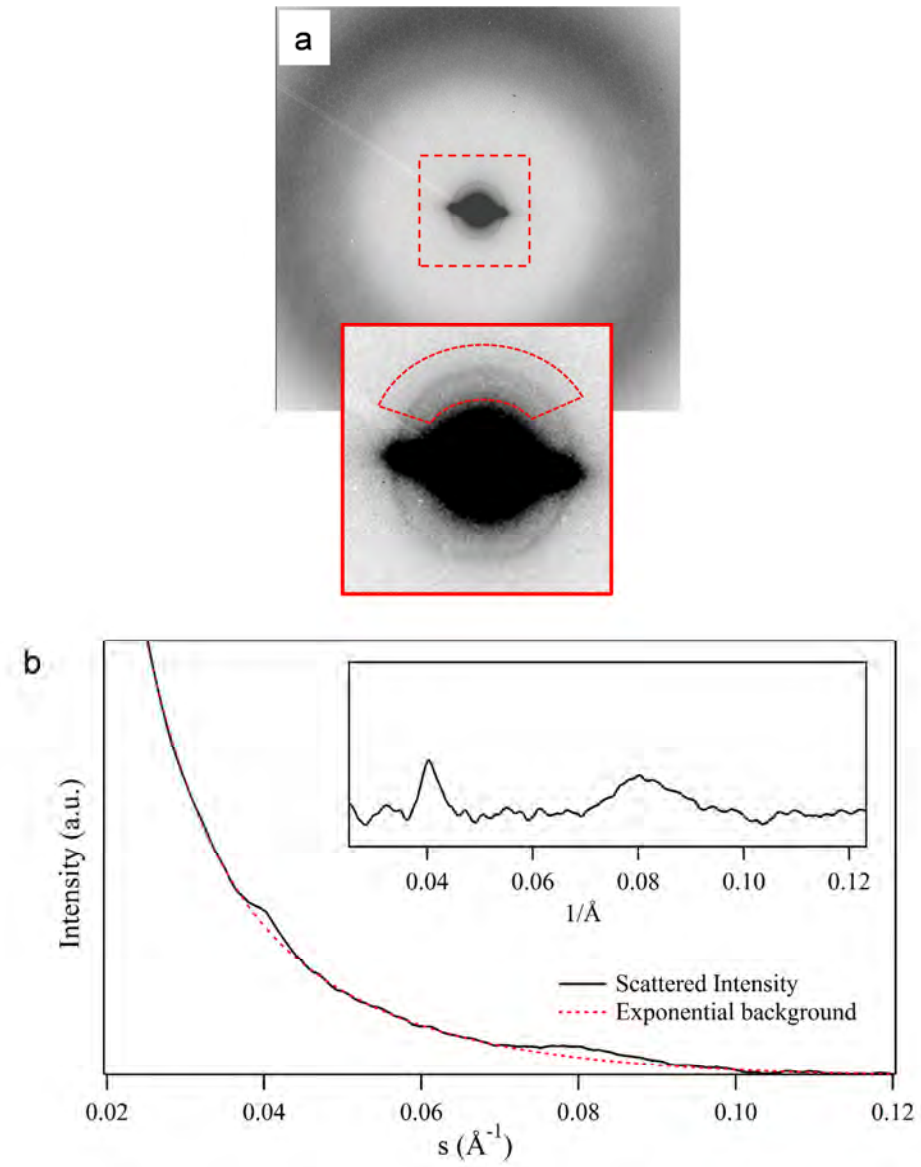

Figure 7. (a) 2D X-ray diffraction pattern of PBTTT/$PC_{71}BM$ (1:1) nanofilaments inside AAO pores of 25 nm diameter. The central area of the pattern has been augmented and shown as inset. (b) 1D intensity profile as a function of the modulus of the scattering vector s, for the PBTTT/$PC_{71}BM$ (1:1) nanofilaments inside AAO pores of 25 nm diameter. As an inset is presented the region of interest of the scattered intensity ones the background has been subtracted.

It is evident that 25 nm AAO pores induce a strong confinement effect to the PBTTT/$PC_{71}BM$ (1:1) structure. On the one hand the degree of crystallinity in the nanofilaments is dramatically reduced and on the other hand it is induced a phase segregation consisting on a fraction of PBTTT crystals with a triclinic unit cell and an amorphous fraction of PBTTT and $PC_{71}BM$. Different factors could explain this behavior: first the spatial constrains inhibit dramatically crystallization, second a small fraction of $PC_{71}BM$ is not infiltrated into the AAO pores remaining amorphous in the residual film (Figure S6) and third the monoclinic unit cell of the bimolecular crystals is larger than the triclinic unit cell of the PBTTT crystals.

Regarding crystal orientation of PBTTT in the blend nanoarray, Figure 8a shows the normalized integrated intensity of the 200 reflection as a function of the azimuthal angle (φ) for the nanofilaments of the blend inside AAO pores of 40 nm and 180 nm diameters, and for the nanofilaments of the homopolymer inside AAO pores of 40 nm diameter for comparison. It is observed that the equatorial intensity maximum centered at $\varphi = 180^{o}$ increases with filament diameter for the blend and it is more prominent for the blend than for the homopolymer filaments with the same diameter.

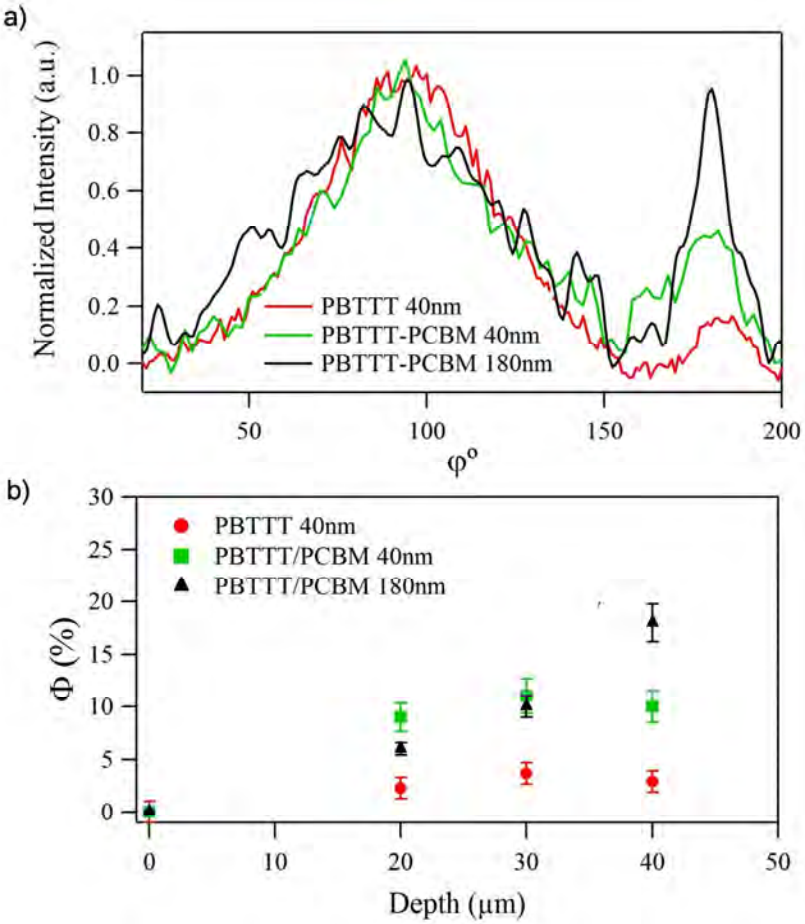

Figure 8. (a) Normalized integrated intensity of the 200 reflection as a function of the azimuthal angle (φ), obtained at equivalent depth (40μm), for the nanofilaments of the homopolymer inside AAO pores of 40 nm diameter (red) and the nanofilaments of the blend inside AAO pores of 40 nm (green) and 180 nm diameter (black). (b) Equatorial oriented fraction as a function of depth for the nanofilaments of the homopolymer inside AAO pores of 40 nm diameter (red) and the nanofilaments of the blend inside AAO pores of 40 nm (green) and 180 nm diameter (black).

The equatorial oriented fraction ($\boldsymbol{\Phi}$) has been calculated by means of $= \boldsymbol{A_{eq}}/(\boldsymbol{A_{eq}} + \boldsymbol{A_{mer}})$, where $\boldsymbol{A_{eq}}$ is the area under the equatorial intensity maximum centered at φ = 180º and $\boldsymbol{A_{mer}}$ is the area under the meridian intensity maximum centered at φ = 90º. Figure 8(b) shows the

equatorial oriented fraction as a function of depth into the nanofilaments. It is seen that there is not equatorial orientation in the residual polymer film outside the AAO membrane for the homopolymer neither for the blend. Going deep into the porous membrane $\boldsymbol{\Phi}$ is larger for the blend than for the homopolymer and it increases with increasing the pore diameter. It is also interesting to point out that for the 40 nm pore diameter $\boldsymbol{\Phi}$ is almost constant with the depth for both the homopolymer and the blend while it increases as a function of depth for the 180 nm pore diameter.

4. Conclusions

In summary, we have proven strong confinement effects on the structural behavior of PBTTT and the photovoltaic blend PBTTT/$PC_{71}BM$ (1:1). The PBTTT nanofilaments crystallize, like the bulk material, in a triclinic unit cell independent of diameter. However, the interaction of the polymer with the pore walls makes the PBTTT crystals partially orient concentric to each other and to the AAO pore axis. The confinement effects are still more pronounced on the PBTTT/$PC_{71}BM$ nanofilaments. While the blend nanofilaments with 180 nm diameter behave like the blend in the bulk, forming a bimolecular crystal with a monoclinic unit cell containing one PBTTT monomer per fullerene molecule, the confinement of PBTTT/$PC_{71}BM$ (1:1) inside AAO pores of 40 nm diameter induces partial phase segregation provoking two different crystal populations: one of them corresponding to PBTTT crystals with a triclinic unit cell and the other corresponding to the co-crystallization of PBTTT and $PC_{71}BM$ within a monoclinic unit-cell. It is also evident that 25 nm AAO porous induce the strongest confinement to the blend structure, reducing the crystallinity in the nanofilaments and inducing a phase segregation consisting on a fraction of PBTTT crystals with a triclinic unit cell and an

amorphous fraction of PBTTT and $PC_{71}BM$. Regarding the orientation of the blend crystals, we have shown that there is an equatorial oriented fraction in the nanofilaments that the bulk material doesn't exhibit. This equatorial oriented fraction increases with filament diameter for the blend and it is more prominent for the blend than for the homopolymer filaments with the same diameter. In conclusion, the important changes in the photovoltaic blend microstructure induced by strong confinement effects may possibly have a significant impact on the final properties of devices where such approaches are implemented.

Acknowledgements

This work is funded by MINECO through projects MAT2014-59187-R and MAT2015-66443-C02 1-R. We thank the ESRF for beamtime at ID13 and M. Burghammer for technical support during our measurements.

Appendix A. Supplementary data

Supplementary data related to this article can be found at

References

[1] S.R. Forrest, The path to ubiquitous and low-cost organic electronic appliances on plastic, Nature 428 (2004) 911.
[2] H. Sirringhaus, 25th Anniversary Article: Organic Field‐Effect Transistors: The Path Beyond Amorphous Silicon, Advanced Materials 26(9) (2014) 1319-1335.
[3] Y. Liu, J. Zhao, Z. Li, C. Mu, W. Ma, H. Hu, K. Jiang, H. Lin, H. Ade, H. Yan, Aggregation and morphology control enables multiple cases of high-efficiency polymer solar cells, Nature Communications 5 (2014) 5293.
[4] H. Yan, Z. Chen, Y. Zheng, C. Newman, J.R. Quinn, F. Dötz, M. Kastler, A. Facchetti, A high-mobility electron-transporting polymer for printed transistors, Nature 457 (2009) 679.

[5] M. Pandey, S.S. Pandey, S. Nagamatsu, S. Hayase, W. Takashima, Solvent driven performance in thin floating-films of PBTTT for organic field effect transistor: Role of macroscopic orientation, Organic Electronics 43 (2017) 240-246.
[6] I. McCulloch, M. Heeney, C. Bailey, K. Genevicius, I. MacDonald, M. Shkunov, D. Sparrowe, S. Tierney, R. Wagner, W. Zhang, M.L. Chabinyc, R.J. Kline, M.D. McGehee, M.F. Toney, Liquid-crystalline semiconducting polymers with high charge-carrier mobility, Nature Materials 5 (2006) 328.
[7] J.E. Parmer, A.C. Mayer, B.E. Hardin, S.R. Scully, M.D. McGehee, M. Heeney, I. McCulloch, Organic bulk heterojunction solar cells using poly(2,5-bis(3-tetradecyllthiophen-2-yl)thieno[3,2,-b]thiophene), Applied Physics Letters 92(11) (2008) 113309.
[8] N.C. Cates, R. Gysel, Z. Beiley, C.E. Miller, M.F. Toney, M. Heeney, I. McCulloch, M.D. McGehee, Tuning the Properties of Polymer Bulk Heterojunction Solar Cells by Adjusting Fullerene Size to Control Intercalation, Nano Letters 9(12) (2009) 4153-4157.
[9] S.N. Patel, A.M. Glaudell, K.A. Peterson, E.M. Thomas, K.A. O'Hara, E. Lim, M.L. Chabinyc, Morphology controls the thermoelectric power factor of a doped semiconducting polymer, Science Advances 3(6) (2017).
[10] J. Xu, S. Wang, G.-J.N. Wang, C. Zhu, S. Luo, L. Jin, X. Gu, S. Chen, V.R. Feig, J.W.F. To, S. Rondeau-Gagné, J. Park, B.C. Schroeder, C. Lu, J.Y. Oh, Y. Wang, Y.-H. Kim, H. Yan, R. Sinclair, D. Zhou, G. Xue, B. Murmann, C. Linder, W. Cai, J.B.-H. Tok, J.W. Chung, Z. Bao, Highly stretchable polymer semiconductor films through the nanoconfinement effect, Science 355(6320) (2017) 59-64.
[11] G. Yu, J. Gao, J.C. Hummelen, F. Wudl, A.J. Heeger, Polymer Photovoltaic Cells: Enhanced Efficiencies via a Network of Internal Donor-Acceptor Heterojunctions, Science 270(5243) (1995) 1789-1791.
[12] Z. He, B. Xiao, F. Liu, H. Wu, Y. Yang, S. Xiao, C. Wang, T.P. Russell, Y. Cao, Single-junction polymer solar cells with high efficiency and photovoltage, Nature Photonics 9 (2015) 174.
[13] J. Zhao, Y. Li, G. Yang, K. Jiang, H. Lin, H. Ade, W. Ma, H. Yan, Efficient organic solar cells processed from hydrocarbon solvents, Nature Energy 1 (2016) 15027.
[14] M.A. Ruderer, P. Muller-Buschbaum, Morphology of polymer-based bulk heterojunction films for organic photovoltaics, Soft Matter 7(12) (2011) 5482-5493.
[15] P.A. Staniec, A.J. Parnell, A.D.F. Dunbar, H. Yi, A.J. Pearson, T. Wang, P.E. Hopkinson, C. Kinane, R.M. Dalgliesh, A.M. Donald, A.J. Ryan, A. Iraqi, R.A.L. Jones, D.G. Lidzey, The Nanoscale Morphology of a PCDTBT:PCBM Photovoltaic Blend, Advanced Energy Materials 1(4) (2011) 499-504.
[16] Á. Rodríguez-Rodríguez, M. Soccio, D.E. Martínez-Tong, T.A. Ezquerra, B. Watts, M.-C. García-Gutiérrez, Competition between phase separation and structure confinement in P3HT/PCDTBT heterojunctions: Influence on nanoscale charge transport, Polymer 77 (2015) 70-78.
[17] N. Seok‐In, K. Seok‐Soon, J. Jang, O. Seung‐Hwan, K. Juhwan, K. Dong‐Yu, Efficient Polymer Solar Cells with Surface Relief Gratings Fabricated by Simple Soft Lithography, Advanced Functional Materials 18(24) (2008) 3956-3963.
[18] D. Chen, W. Zhao, T.P. Russell, P3HT Nanopillars for Organic Photovoltaic Devices Nanoimprinted by AAO Templates, ACS Nano 6(2) (2012) 1479-1485.
[19] T. Pfadler, M. Coric, C.M. Palumbiny, A.C. Jakowetz, K.-P. Strunk, J.A. Dorman, P. Ehrenreich, C. Wang, A. Hexemer, R.-Q. Png, P.K.H. Ho, P. Müller-Buschbaum, J. Weickert, L.

Schmidt-Mende, Influence of Interfacial Area on Exciton Separation and Polaron Recombination in Nanostructured Bilayer All-Polymer Solar Cells, ACS Nano 8(12) (2014) 12397-12409.
[20] Á. Rodríguez-Rodríguez, E. Rebollar, M. Soccio, T.A. Ezquerra, D.R. Rueda, J.V. Garcia-Ramos, M. Castillejo, M.-C. Garcia-Gutierrez, Laser-Induced Periodic Surface Structures on Conjugated Polymers: Poly(3-hexylthiophene), Macromolecules 48(12) (2015) 4024-4031.
[21] J. Cui, Á. Rodríguez-Rodríguez, M. Hernández, M.-C. García-Gutiérrez, A. Nogales, M. Castillejo, D. Moseguí González, P. Müller-Buschbaum, T.A. Ezquerra, E. Rebollar, Laser-Induced Periodic Surface Structures on P3HT and on Its Photovoltaic Blend with PC71BM, ACS Applied Materials & Interfaces 8(46) (2016) 31894-31901.
[22] Á. Rodríguez-Rodríguez, E. Rebollar, T.A. Ezquerra, M. Castillejo, J.V. Garcia-Ramos, M.-C. García-Gutiérrez, Patterning Conjugated Polymers by Laser: Synergy of Nanostructure Formation in the All-Polymer Heterojunction P3HT/PCDTBT, Langmuir 34(1) (2018) 115-125.
[23] S. Martin, W.R. B., G. Ulrich, W.J. H., Nanotubes by Template Wetting: A Modular Assembly System, Angewandte Chemie International Edition 43(11) (2004) 1334-1344.
[24] J. Martín, C. Mijangos, Tailored Polymer-Based Nanofibers and Nanotubes by Means of Different Infiltration Methods into Alumina Nanopores, Langmuir 25(2) (2009) 1181-1187.
[25] M.-C. García-Gutiérrez, A. Linares, J.J. Hernández, D.R. Rueda, T.A. Ezquerra, P. Poza, R.J. Davies, Confinement-Induced One-Dimensional Ferroelectric Polymer Arrays, Nano Letters 10(4) (2010) 1472-1476.
[26] Y. Yao, H.-J. Butt, J. Zhou, M. Doi, G. Floudas, Capillary Imbibition of Polymer Mixtures in Nanopores, Macromolecules 51(8) (2018) 3059-3065.
[27] C. Riekel, M.C. García Gutiérrez, A. Gourrier, S. Roth, Recent synchrotron radiation microdiffraction experiments on polymer and biopolymer fibers, Analytical and Bioanalytical Chemistry 376(5) (2003) 594-601.
[28] H. Inouye, F.-H. Kuo, A.R. Denninger, B. Weinhausen, M. Burghammer, D.A. Kirschner, Myelin structure in unfixed, single nerve fibers: Scanning X-ray microdiffraction with a beam size of 200nm, Journal of Structural Biology 200(3) (2017) 229-243.
[29] J.W.P. Schmelzer, A.S. Abyzov, Thermodynamic analysis of nucleation in confined space: Generalized Gibbs approach, The Journal of Chemical Physics 134(5) (2011) 054511.
[30] H. Wu, Y. Higaki, A. Takahara, Molecular self-assembly of one-dimensional polymer nanostructures in nanopores of anodic alumina oxide templates, Progress in Polymer Science 77 (2018) 95-117.
[31] H. Duran, M. Steinhart, H.-J. Butt, G. Floudas, From Heterogeneous to Homogeneous Nucleation of Isotactic Poly(propylene) Confined to Nanoporous Alumina, Nano Letters 11(4) (2011) 1671-1675.
[32] G. Shi, G. Liu, C. Su, H. Chen, Y. Chen, Y. Su, A.J. Müller, D. Wang, Reexamining the Crystallization of Poly(ε-caprolactone) and Isotactic Polypropylene under Hard Confinement: Nucleation and Orientation, Macromolecules 50(22) (2017) 9015-9023.
[33] M. Steinhart, P. Göring, H. Dernaika, M. Prabhukaran, U. Gösele, E. Hempel, T. Thurn-Albrecht, Coherent Kinetic Control over Crystal Orientation in Macroscopic Ensembles of Polymer Nanorods and Nanotubes, Physical Review Letters 97(2) (2006) 027801.
[34] S. Himmelberger, J. Dacuña, J. Rivnay, L.H. Jimison, T. McCarthy-Ward, M. Heeney, I. McCulloch, M.F. Toney, A. Salleo, Effects of Confinement on Microstructure and Charge Transport in High Performance Semicrystalline Polymer Semiconductors, Advanced Functional Materials 23(16) (2013) 2091-2098.

[35] F. Dou, E. Buchaca-Domingo, M. Sakowicz, E. Rezasoltani, T. McCarthy-Ward, M. Heeney, X. Zhang, N. Stingelin, C. Silva, The effect of phase morphology on the nature of long-lived charges in semiconductor polymer:fullerene systems, Journal of Materials Chemistry C 3(15) (2015) 3722-3729.
[36] D.E. Markov, C. Tanase, P.W.M. Blom, J. Wildeman, Simultaneous enhancement of charge transport and exciton diffusion in poly(p-phenylene vinylene) derivatives, Physical Review B 72(4) (2005) 045217.
[37] M.-C. Garcia-Gutierrez, A. Linares, I. Martin-Fabiani, J.J. Hernandez, M. Soccio, D.R. Rueda, T.A. Ezquerra, M. Reynolds, Understanding crystallization features of P(VDF-TrFE) copolymers under confinement to optimize ferroelectricity in nanostructures, Nanoscale 5(13) (2013) 6006-6012.
[38] H.-L. Yi, C.-C. Hua, PBTTT-C16 sol-gel transition by hierarchical colloidal bridging, Soft Matter 14(7) (2018) 1270-1280.
[39] M.L. Chabinyc, M.F. Toney, R.J. Kline, I. McCulloch, M. Heeney, X-ray Scattering Study of Thin Films of Poly(2,5-bis(3-alkylthiophen-2-yl)thieno[3,2-b]thiophene), Journal of the American Chemical Society 129(11) (2007) 3226-3237.
[40] A. Hammersley, FIT2D Website. http://www.esrf.eu/computing/scientific/FIT2D (2010).
[41] I. Martín-Fabiani, M.-C. García-Gutiérrez, D.R. Rueda, A. Linares, J.J. Hernández, T.A. Ezquerra, M. Reynolds, Crystallization under One-Dimensional Confinement in Alumina Nanopores of Poly(trimethylene terephthalate) and Its Composites with Single Wall Carbon Nanotubes, ACS Applied Materials & Interfaces 5(11) (2013) 5324-5329.
[42] E. Cho, C. Risko, D. Kim, R. Gysel, N. Cates Miller, D.W. Breiby, M.D. McGehee, M.F. Toney, R.J. Kline, J.-L. Bredas, Three-Dimensional Packing Structure and Electronic Properties of Biaxially Oriented Poly(2,5-bis(3-alkylthiophene-2-yl)thieno[3,2-b]thiophene) Films, Journal of the American Chemical Society 134(14) (2012) 6177-6190.
[43] N.C. Miller, E. Cho, M.J.N. Junk, R. Gysel, C. Risko, D. Kim, S. Sweetnam, C.E. Miller, L.J. Richter, R.J. Kline, M. Heeney, I. McCulloch, A. Amassian, D. Acevedo-Feliz, C. Knox, M.R. Hansen, D. Dudenko, B.F. Chmelka, M.F. Toney, J.-L. Brédas, M.D. McGehee, Use of X-Ray Diffraction, Molecular Simulations, and Spectroscopy to Determine the Molecular Packing in a Polymer-Fullerene Bimolecular Crystal, Advanced Materials 24(45) (2012) 6071-6079.

- Solution template wetting allows the fabrication of polymer and hybrid nanowires.
- Confinement in PBTTT and PBTTT/PCBM nanowires has been studied by X-ray nanoprobes.
- Confinement induces phase segregation and different crystal forms in hybrid nanowires.
- Interaction of organic semiconductors with template walls directs the overall texture.